The Journal of Chemical Physics

A structural indicator for water built upon potential energy considerations

Cite as: J. Chem. Phys. **152**, 244503 (2020); https://doi.org/10.1063/5.0010895
Submitted: 15 April 2020 • Accepted: 08 June 2020 • Published Online: 25 June 2020

Joan M. Montes de Oca, Francesco Sciortino and Gustavo A. Appignanesi

The Journal of Chemical Physics ARTICLE scitation.org/journal/jcp

A structural indicator for water built upon potential energy considerations

Cite as: J. Chem. Phys. 152, 244503 (2020); doi: 10.1063/5.0010895
Submitted: 15 April 2020 • Accepted: 8 June 2020 •
Published Online: 25 June 2020

Joan M. Montes de Oca,[1] Francesco Sciortino,[2] and Gustavo A. Appignanesi[3,a)]

AFFILIATIONS

[1] Pritzker School of Molecular Engineering, University of Chicago, Chicago, Illinois 60637, USA
[2] Dipartimento di Fisica, Sapienza Universitá di Roma, Piazzale A. Moro 5, Roma 00185, Italy
[3] INQUISUR, Departamento de Química, Universidad Nacional del Sur (UNS)-CONICET, Avenida Alem 1253, 8000 Bahía Blanca, Argentina

[a)] **Author to whom correspondence should be addressed:** appignan@criba.edu.ar

ABSTRACT

We introduce a parameter-free structural indicator to classify local environments of water molecules in stable and supercooled liquid states, which reveals a clear two-peak distribution of local properties. The majority of molecules are tetrahedrally coordinated (T molecules), via low-energy hydrogen bonds. The minority component, whose relative concentration decreases with a decrease in the temperature at constant pressure, is characterized by prevalently three-coordinated molecules, giving rise to a distorted local network around them (D molecules). The inter-conversion between T and D molecules explains the increasing specific heat at constant pressure on cooling. The local structure around a T molecule resembles the one found experimentally in low-density amorphous ice (a network structure mostly composed by T molecules), while the local structure around a D molecule is reminiscent of the structural properties of high-density amorphous ice (a network structure composed by a mixture of T and D molecules).

I. INTRODUCTION

Despite its molecular simplicity, water presents a profuse number of thermodynamic and dynamic anomalies in both the normal liquid and the supercooled regime. These anomalies play an important role in a wide range of disciplines, including meteorology, materials science, and biology.[1–9] Anomalies also extend to the non-equilibrium phases of water. Specifically, water presents at least two amorphous structures with quite different local arrangements: the low-density amorphous (LDA) ice and the high-density amorphous (HDA) ice.[3,10] A two-liquid scenario has been proposed as a plausible explanation for the existence of two glass states, as well as for the thermodynamic anomalies.[6] In this scenario, the HDA–LDA coexistence line continues in the liquid regime until ending at a liquid–liquid critical point. These two liquid phases are expected to arise from the competition of two local molecular arrangements differing in entropy, volume, and enthalpy.[6,11] The low-density liquid is described as consisting of an open network of tetrahedrally coordinated molecules [each molecule being engaged in four low-energy linear hydrogen bonds (HBs)], while in the higher-density liquid, the tetrahedral order is expected to be partially distorted by one or more additional water neighbors in the first coordination shell. Computational[12–16] and experimental[17–22] evidence has been found in favor of the existence of these two liquid phases, yet it has been difficult to determine the precise nature and relative abundance of the underlying local molecular arrangements, particularly in the liquid regime where thermal distortion hinders a proper local structural classification. To reach consensus on the presence of two well-defined local environments in water,[23] it is necessary to find an order parameter capable of producing a clear *two-peak* distribution, even far from the expected location of the liquid–liquid critical point.

Several structural indicators have been proposed in the past,[24] mostly based on the analysis of simulated configurations and built upon structural traits capable of discerning molecules with well-ordered or distorted local arrangements.[8,25–37] One of these indicators, the widely used local structure index (LSI),[28–31] quantifies the degree of translational order up to the second molecular shell. The LSI is based on the knowledge that tetrahedral molecules present a clear gap between the first and second molecular shells. The more

recent ζ index, introduced by Russo and Tanaka,[8,36] also focuses on the local translational order while additionally considering hydrogen bonding in an explicit way. Both indicators display distribution functions, which can be represented as a sum of two limiting distributions, which suggest a crossover between the two forms on cooling or varying pressure. The LSI is the only indicator that displays neat bimodal distributions for the different water models, but only if the analysis is performed in the inherent structures[38,39] (IS). One drawback of the LSI indicator is that the relative areas of the two limiting distributions depend on the arbitrary threshold implied in the index definition (r_{th}, the region of the inter-shell gap in the radial distribution function, which is considered for the calculation).

Here, we investigate a novel clear-cut *parameter-free* structural indicator for water, built not upon structural preconceptions, but, instead, upon potential energy considerations. This new order parameter provides neat bimodal distributions in both the normal liquid and in the supercooled regimes, overcoming the inability of all former order parameters to accurately classify water molecules within two kinds of species. An analysis of the inherent structure configurations, which suppress the thermal distortions of the real dynamics (RD) and facilitate the identification of inter-particle bonds,[40] shows that one class of molecules are mostly tetrahedrally coordinated molecules (T), while the other class of molecules have a more distorted network of hydrogen bonds in the first coordination shell (D). Interestingly, we find that the radial distribution function for T and D resembles the radial distribution function of LDA and HDA, suggesting that the supercooled liquid adopts configurations that correspond to the thermally distorted versions of the underlying amorphous structures. Moreover, the temperature dependence of T and D proportions suggests that the low-density liquid might be composed almost exclusively of T, while the high-density phase might be a state in which T molecules surround a small percentage of D. Finally, we show that the rate of T-D inter-conversion on cooling is responsible for the increase in the heat capacity of water.

II. METHODS

We investigate two different water models, SPCE[41] and TIP4P/2005,[42] each of them at two different pressures (P) for several temperatures. The simulations are performed with GROMACS Version 5.1.1, for a system of $N = 4420$ particles. Minimization is performed with the steepest descent algorithm implemented in GROMACS (steep) until convergence to a maximum force of 10.0 kJ mol^{-1} nm^{-1} acting over any atom. For each water molecule i, we evaluate all pairwise interactions V_{ij}, $j \neq i$, and sort them according to their intensity, from the smallest to the largest value. We then define $V_4(i)$, the forth V_{ij}. If a molecule forms four strong linear HBs, $V_4(i)$ is expected to be of the order of the linear HB energy. Perturbing the tetrahedral shell inevitably produces a distortion of at least one of the four HBs, resulting in a larger $V_4(i)$ value. For all-purpose of this work, T molecules are defined as those with $V_4(i) \leq -12$ kJ mol^{-1} calculated over the inherent structures. We note that setting a classification threshold at -12 kJ mol^{-1} could be seen as arbitrary, but we have selected this threshold because the $V_4(i)$ distribution displays a clear minimum at that point. We point out that while the classification method can be subject to the threshold definition, the structural index itself remains parameter-free. We will also discuss the distribution of $V_5(i)$, the fifth V_{ij}, and compare it with the $V_4(i)$ one.

III. RESULTS AND DISCUSSION

Figures 1(a) and 1(b) display the distribution of V_4, $P(V_4)$, for SPC/E and TIP4P/2005 water for a series of temperatures, both for the instantaneous and for the IS configurations. V_4 produces very clear two-peak distributions for the two schemes and both models. The energy minimization shifts the low-energy peak to lower interaction values, while leaving the position of the higher-energy peak unaffected. The low-energy peak (the T-peak) is centered on the typical value of a linear HB, while the high-energy peak (the D-peak) indicates a significant distortion of the linear geometry, suggesting that the optimal tetrahedral bonding geometry has been disturbed. Such bimodal behavior clearly indicates that distinct molecular local structures exist that inter-convert in time and whose concentration varies as the temperature is altered. At variance from other structural indicators,[30,31,33,34] the V_4 distribution is bimodal both at the real dynamics and at the inherent structures. Recall that the inherent structure describes the reference configuration in the absence of thermal fluctuations.[38,39] Indeed, the minimization procedure, following a steepest descent path on the potential energy landscape, brings the real-dynamic configuration to its closest local minimum, eliminating the blurring effect of thermal fluctuations that affect the real dynamics. In the case of water, thermal fluctuations (hindered translation and hindered rotations) significantly alter the geometry of the inherent structure, masking the correct identification of the particles and, even more, the proper identification of hydrogen bonds.[43] Data in Fig. 1(a) show that the minimization process results in a better resolved two-peak structure and a clear identification of the molecule type. It is worth noting that a change from the inherent structure to the real dynamic would cause a significant number of molecules classified as T to migrate under the D-peak. We will, later, show that the inherent structures not only display a better-resolved bimodal distribution but also provide with two molecular categories able to rationalize the increase in the specific heat on cooling.

Figure 1(c) shows the temperature dependence of the fraction of T molecules. Unlike most local order parameter predictions, according to the V_4 classification introduced here, the T component is predominant at all the temperatures we tested. This result supports a description of ambient pressure water as a tetrahedral network with a small concentration of defects.[44] We note that the previously introduced molecular classification, other than the V_4 index, suggests a significantly larger concentration of unstructured molecules.

Figure 1(d) shows $-k_B T P(V_4)$, where k_B is the Boltzmann constant. This quantity provides the free-energy profile as a function of V_4, where the two free-energy basins associated with D and T configurations emerge. The T-basin becomes deeper and deeper on cooling, consistent with the increasing thermodynamic stability of the T molecules on cooling. Finally, Figs. 1(e) and 1(f) show the distribution of the total potential energy in IS and RD,

$$E_i = \frac{1}{2} \sum_{j \neq i} V_{ij}, \tag{1}$$

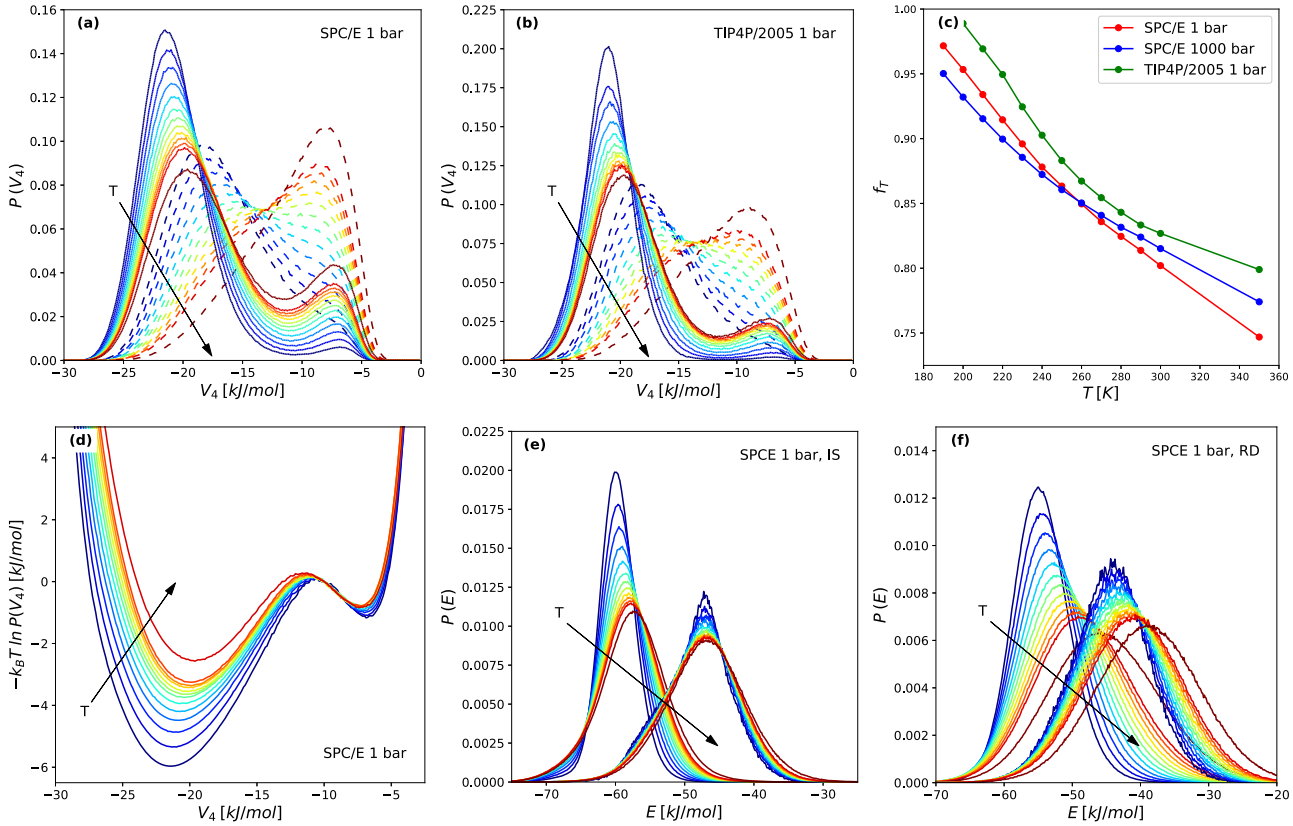

FIG. 1. V_4 for SPC/E (a) and TIP4P/2005 (b) both for equilibrium configurations or real dynamics (RD, dashed lines) and for inherent-structures (IS, full lines) at 1 bar. The temperature ranges are as follows: SPC/E: T from 190 K to 300 K in 10 K steps and 350 K; TIP4P/2005: 210–310 in 10 K steps plus 350 K. (c) Temperature dependence of the fraction of T molecules f_T. (d) Free-energy profile associated with the distribution $P(V_4)$ evaluated in the IS for SPC/E at 1 bar, signaling a progressive increase in the thermodynamic stability of the T molecules. (e) Distribution of the IS total energy per particle E for both T and D molecules. Note that (i) the distributions for T and D molecules are quite well separated by more than 10 kJ/mol and (ii) the D distribution does not change significantly with temperature. The arrows depict the direction of increasing temperature. (f) Similar to that in (e) but for equilibrium configurations (RD).

separated by classes, for the SPC/E water model (see the supplementary material, Fig. S1 for TIP4P/2005). D and T are characterized by a significantly different average potential energy, once again highlighting the ability of V_4 to differentiate the subtle diversity of the local structures observed in liquid water.

Before proceeding to the detailed analysis of the distinctive features of the two molecular arrangements mentioned above, we attempt to correlate V_4 with the number of HB in which a molecule is involved. We are guided also by a recent, interesting work that studied the relevance of molecules with a different number of HBs in deep supercooled states.[44] We, thus, classify molecules according to the number of HB they participate in (three, four, or five), by using the standard geometric HB criterion (an O–O distance of less than 3.4 Å and a $H\hat{O}O$ angle less than 30°) evaluated at the inherent configurations. Figure 2(a) shows the fraction of three-coordinated, four-coordinated, or five-coordinated molecules as a function of temperature for SPC/E at ambient pressure (here, we use the term n-coordinated molecule to refer to molecules with n HBs). The number of tetra functional particles approaches one on cooling, consistent with the idea that hyper-quenched water forms a defect free random tetrahedral network (LDA). The fraction of tri-coordinated molecules is larger than the fraction of five-coordinated molecules. The left inset in Fig. 2(a) shows the difference between the fraction of three and five HB coordinated molecules. At deep supercooled temperatures, this difference vanishes, suggesting that the energetic cost of wasting an HB becomes unsustainable such that all protons must participate in an HB. This forces the number of five-coordinated and three-coordinated molecules to become equal. The right inset shows the fraction of double HB donors among tri-coordinated molecules, suggesting that double-donor D molecules are progressively more stable than double-acceptors while decreasing the temperature.

The different local structures associated with the different number of HBs show up also in the particle potential energy. To look for the correlation between structural and energetic properties, we present, in Fig. 2(b), a plot of V_5 vs V_4, also classifying molecules with different hydrogen bond coordinations (as defined by the geometric criterion). From this figure, we can note that

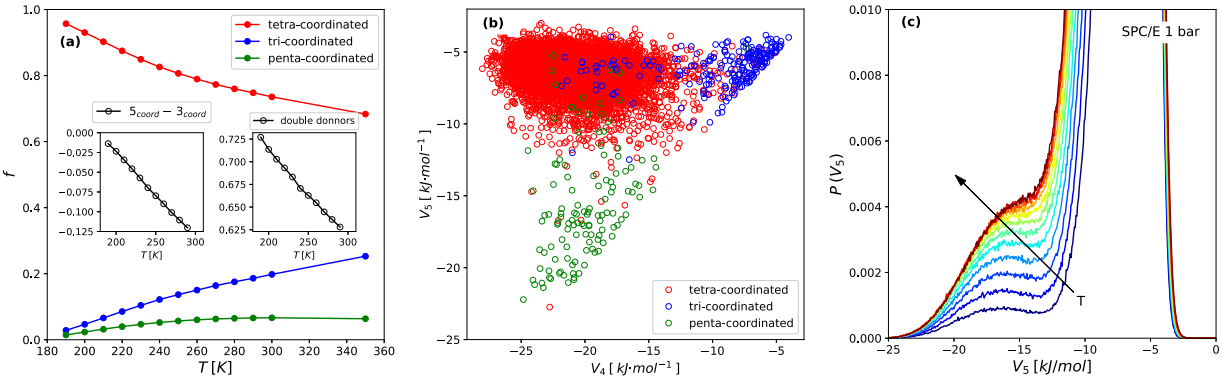

FIG. 2. (a) Temperature dependence of the fractions of penta-coordinated, tetra-coordinated, and tri-coordinated molecules for SCP/E water at P = 1 bar. The inset on the left shows the difference in the fraction of penta-coordinated and tri-coordinated molecules. This number approaches zero on cooling. The inset on the right shows the temperature dependence of the fractions of double-donors among tri-coordinated molecules. (b) Parametric V_4 vs V_5 scatter plot for a single configuration of SPC/E water at T = 190 K; each symbol corresponds to a molecule, and it is colored according to the number of geometrically defined hydrogen bonds (5HB, green; 4HB, red; and 3HB, blue). (c) V_5 distribution for SPC/E at P = 1 bar.

tetra-coordinated molecules, indeed, possess a low V_4 value (a strong fourth interaction compatible with a good-quality hydrogen bond) and a high V_5 (the fifth neighbor in energy interacts with a poor interaction value), while most of the tri-coordinated molecules do have large values both in V_4 and V_5 (poor interactions). Five-coordinated molecules are predominantly characterized by both low V_4 and V_5. A few out-layers are found, as always expected when a sharp cut-off is used in a continuous distribution, a typical weakness of the geometric criteria.

Figure 2(b) also shows that a projection of the scatter plot on the V_4 axis allows us to identify the molecules in the small-amplitude peak of P(V_4) as three-coordinated molecules, while the large-amplitude peak of P(V_4), for small V_4 values, receives contributions both from four-coordinated and five-coordinated molecules. A projection on the V_5 axis would provide complementary information, separating the five-coordinated from the four-coordinated ones. However, as depicted in Fig. 2(c), the V_5 probability distribution does not display a well-separated peak as found in the previous V_4 distributions, but instead, a low-energy shoulder.

An important message from this analysis is that over-coordinated molecules appear to play a role at very low temperatures, mostly compensating the existence of under-coordinated defects. At the same time, their small concentration compared to the four-coordinated ones does not significantly alter the properties of the molecules associated with the low V_4 peak in the overall structural or thermodynamic behavior. Thus, from now on, we will just consider T and D molecules as defined solely by the V4 distribution (as carried out in Fig. 1).

To investigate the local molecular arrangements around T and D particles we evaluate the oxygen–oxygen radial distribution functions (RDF) and separate it according to

$$g(r) = f_T g_T(r) + (1 - f_T) g_D(r), \tag{2}$$

where in the $g_T(r)$ and $g_D(r)$, the molecule in the origin is a T and a D, respectively, and f_T is the fraction of T molecules. Here, f_T, $g_T(r)$, and $g_D(r)$ depend on temperature. For the computation of the RDF, we classify the molecules at the IS level, but use equilibrium configurations (real dynamic configurations) to evaluate the relative distances. Figure 3 shows $g_T(r)$ and $g_D(r)$ at ambient pressure, and T = 210 K for the SPC/E water model. $g_T(r)$ presents a clear separation between the first and second coordination shells (the two first peaks). On the other hand, $g_D(r)$ shows a broad-peak centered around 3.5 Å, which overlaps with the linear HB peak centered at

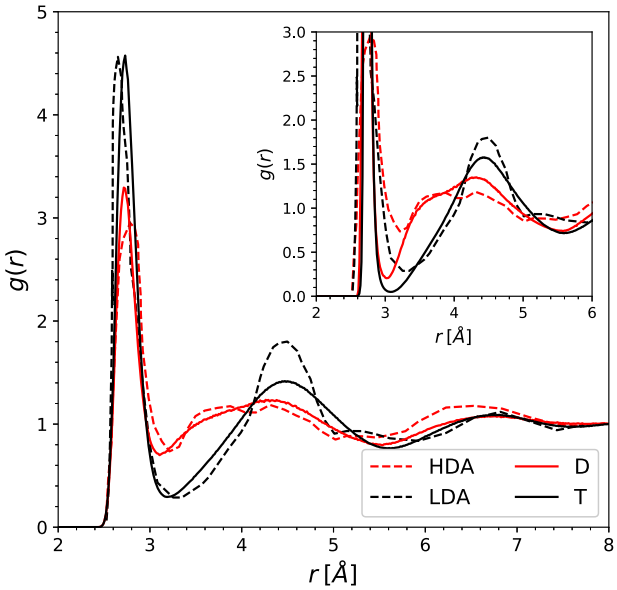

FIG. 3. Oxygen–oxygen radial distribution functions (RDF) separated into two components according to the identity (T or D) of the molecule located at the origin calculated for the SPC/E model (see the supplementary material, Fig. S2 for TIP4P/2005) in the real dynamic (main) and inherent structures (inset). The temperature and pressure were 210 K and 1 bar, respectively. Experimental HDA and LDA were reported to be obtained at 80 K.[45]

2.7 Å. The broad-peak suggests the presence of interstitial molecules (molecules that intrude the inter-shell gap and perturb the first coordination shell). Figure 3 shows also the experimental RDFs[45] for the amorphous solid ices HDA and LDA. Remarkable similarities of D and T with HDA and LDA, respectively, are evident. This resemblance has not been obtained so far for any other water structural indicator and suggests that the liquid configurations are thermally deformed relatives of the corresponding amorphous solid structures. In other words, the HDL-LDL equilibrium would be a thermally distorted version of the HDA–LDA equilibrium.

As shown in Fig. 1(c), even well above the melting temperature, the T molecules are the most abundant. This means that the RDF for the T molecules shown in Fig. 3 comes from having a T molecule surrounded by mostly other T molecules (almost a pure T-state at low temperatures). It is more difficult to interpret the D-RDF. Further splitting of the $g(r)$ into components g_{TT}, g_{DD}, and g_{TD} (see the supplementary material, Figs. S3 and S4) and evaluating the number of T or D neighbors surrounding a T or a D molecule confirm that, at low temperatures, most of the T molecules are surrounded by other T molecules, while the small number of D molecules are surrounded by three T molecules in well-defined HB configurations and by T and D molecules at further distances. Thus, while T and D molecules indicate two different molecular arrangements, the LDA-like state is expected to be virtually purely composed of T molecules, while the HDA-like state consists of a mixture of T and D molecules. This strongly confirms that a proper two-state picture of water should not be based on single-molecule properties but, instead, on two different local multi-molecule environments: one almost purely tetrahedral (only T) and one distorted (T and D).

To make this observation more precise, we calculate the total correlation function[46] $h_{DD}(r)$ of the D molecules, $h_{DD}(r) \equiv g_{DD}(r) - 1$, a quantity that should ideally be zero for r larger than the excluded volume if D molecules are randomly distributed in space. As shown in Fig. 4(a), even when the concentration of D molecules is very small (2%–3% of the total number of molecules) in the region below 4.5 Å, $h(r)$ is quite different from zero, strongly indicating a spatial correlation between the D molecules. Additionally, we discover [see Fig. 4(b)] that for distances up to 4 Å, the r dependence of $h(r, T)$ is identical for all temperatures, i.e., a factorization of $h_{DD}(r, T)$ in the product of a function of r ($h^c_{DD}(r)$) times a function of temperature ($\alpha(T)$) ($h_{DD}(r, T) = \alpha(T)h^c_{DD}(r)$). Figure 4(c) provides a hint of this unexpected finding by showing the spatial location of the D molecules at a low temperature for a typical configuration. Most of the D molecules are isolated and randomly dispersed in space, but a non-negligible fraction of D molecules, instead, clusters, providing a non-zero contribution to $h(r)$. Indeed, splitting D molecules in isolated monomers m and clusters, one can write, at low concentrations (defining $f_m \equiv \frac{N^m_D}{N^m_D + N^c_D}$, the fraction of D in monomer state),

$$g_{DD}(r, T) = f_m g^m_{DD}(r, T) + (1 - f_m) g^c_{DD}(r) \tag{3}$$

and assuming ideal gas conditions for the monomers ($g^m_{DD}(r, T) = 1$),

$$\begin{aligned} h_{DD}(r, T) &= f_m + (1 - f_m) g^c_{DD}(r) - 1 \\ &= (1 - f_m) h^c_{DD}(r) = \alpha(T) h^c_{DD}(r), \end{aligned} \tag{4}$$

where, by writing $\alpha(T) \equiv 1 - f_m$, the separation between temperature and radial dependence becomes explicit.

The function $h^c_{DD}(r)$ is characterized by a peak at the HB distance 2.8 Å, followed by a broad secondary peak at 3.5 Å, which decays very slowly with r, confirming that D pairs can bind both by a linear HB and be coordinated at the distorted-network distance of 3.5 Å. In fact, by inspecting all the partial RDFs (see the supplementary material, Fig. S3), it became evident that only a D molecule can be at the characteristic distance of 3.5 Å from any other molecule.

It is worth mentioning that, at variance of D molecules, over-coordinated molecular defects show radial distribution functions that do not significantly differ from those displayed by T molecules (see the supplementary material, Fig. S10).

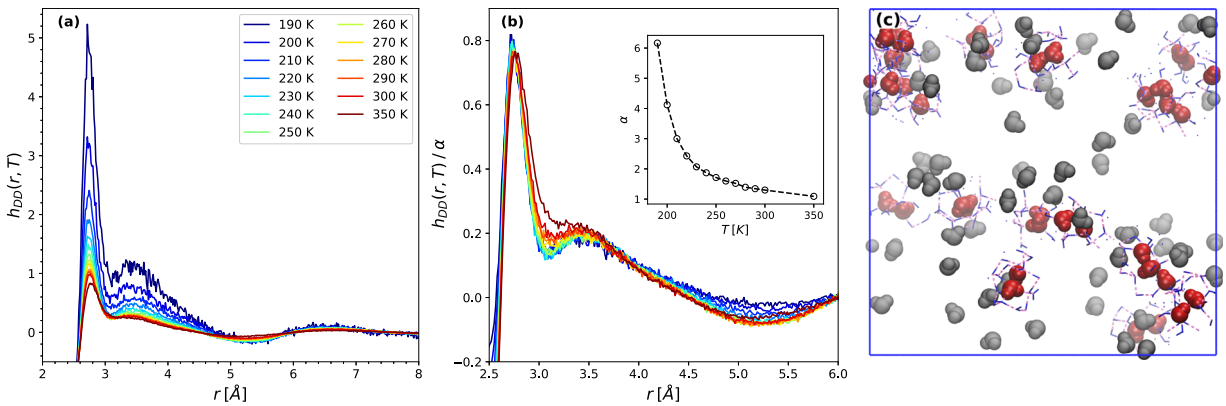

FIG. 4. (a) Total correlation function $h_{DD}(r, T)$. (b) Scaled total correlation function $\alpha(T)h^c_{DD}(r)$, with the resultant scaling factor with temperature (inset). (c) Representation of a typical configuration of SPC/E water at 180 K and ambient pressure, showing the clustering of the D molecules. Red molecules are D molecules with at least one other D molecule within 4 Å, while gray molecules are isolated D molecules (the next D molecule is more than 4 Å away) (see the supplementary material, Figs. S8 and S9 for TIP4P/2005 equivalent figures).

To provide evidence that the classification of the molecules in T and D components also has a thermodynamic relevance, we evaluate the specific heat C_p at constant pressure P as the temperature derivative of the enthalpy H. C_p has two components related to the derivative of the average kinetic and potential energy $K + E$ and the temperature derivative of the volume, this last contribution being negligible compared to the first one (see the supplementary material, Fig. S5). Focusing on the temperature-derivative of E, one can, thus, write, for the excess part of the specific heat,

$$C_p^{ex} \approx \frac{\partial E}{\partial T} = \frac{\partial [f_T E_T + (1 - f_T) E_D]}{\partial T}, \tag{5}$$

where E_T and E_D indicate, respectively, the average potential energy of the two classes of molecules. Then,

$$C_p^{ex} \approx f_T C_p^{T,ex} + (1 - f_T) C_p^{D,ex} + (E_T - E_D) \frac{\partial f_T}{\partial T}. \tag{6}$$

Figure 5 provides a plot of C_p^{ex}, $C_p^{T,ex}$, and $C_p^{D,ex}$. For both water models (see the supplementary material, Fig. S6) and isobars, $C_p^{T,ex}$ and $C_p^{D,ex}$ are weakly temperature dependent and smaller than the system C_p^{ex}, indicating that the temperature dependence of C_p^{ex} arises mostly from the conversion between T and D molecules ($\frac{\partial f_T}{\partial T}$). Accordingly, Fig. 5(b) shows that we can recover the system C_p^{ex} from Eq. (6), taking C_p^{ex} for each individual molecular species from Fig. 5(a), confirming the crucial role of the $\frac{\partial f_T}{\partial T}$ term. Any attempt to obtain a similar behavior in C_p^{ex} based on a different classification of molecular species fails to separate the contribution to C_p^{ex} of each kind of molecule. Particularly, LSI overestimates the fraction of "unstructured" molecules (see the supplementary material, Fig. S7, showing that C_p^{ex} of the unstructured molecules is identical to the system C_p^{ex}).

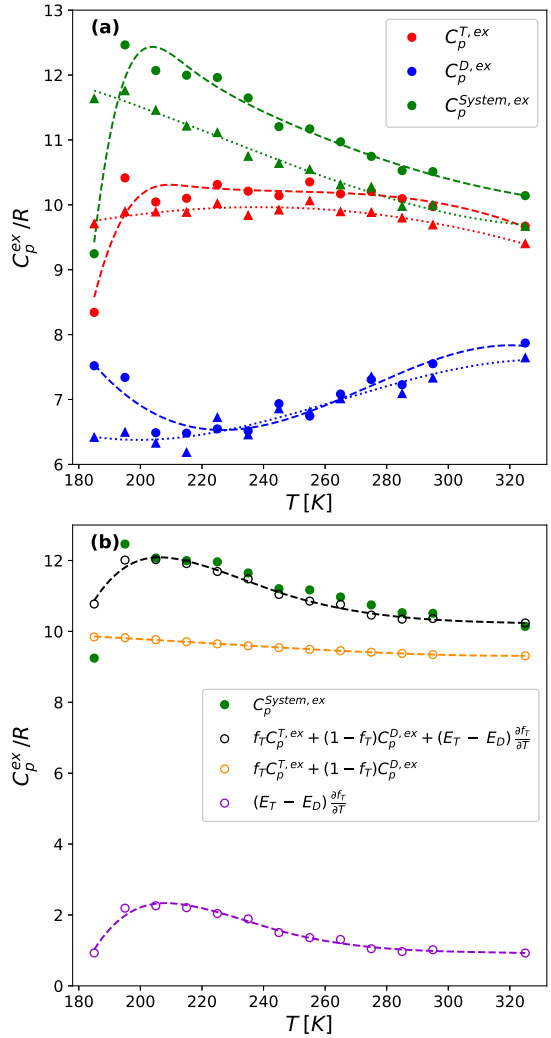

FIG. 5. Excess heat capacity: (a) C_p^{ex} calculated for the SPC/E model at P = 1 bar (filled circles) and P = 1000 bars (up-triangles). Green markers show the C_p^{ex} for the entire system, while red and blue symbols represent the C_p^{ex} obtained for molecules classified as T and D, respectively. (b) T and D inter-conversion contribution to C_p^{ex}: The solid green symbols represent the C_p^{ex} of the entire system directly calculated from the MD at P = 1 bar [$C_p^{system,ex}$in (a)], while the empty black symbols amount to the recovered C_p^{ex} of the system from the contribution of each species C_p^{ex} [$C_p^{ex,T}$and $C_p^{ex,D}$ in (a); orange] and the conversion between T and D molecules (violet empty circles). Symbols correspond to the results of a first-degree finite-difference calculation [as in Eq. (5)], while dashed lines show a cubic spline interpolation of the data, only meant as a guide for the eye.

IV. CONCLUSIONS

In summary, our work shows that it is possible to find a *parameter-free* quantity (V_4) that allows us to detect two clearly different populations of water molecules that inter-convert as temperature is varied: A population composed essentially of water molecules forming three HBs and a population mostly composed by tetrahedrally coordinated molecules (with a quite minor contribution of the five-coordinated one). The two structures are quite distorted by hindered translational and rotational motion, but become clearly resolved when studied in the inherent-structure configurations. Using this classification, water can be described by a random tetrahedral network composed of T molecules with a relatively small number of D molecules (network defects). Interestingly, the structure of the network around a T molecule resembles the structure of LDA, while the structure of the network around a D molecule is similar to HDA. We stress that HDA should not be considered as composed by only D molecules, since a D molecule is surrounded mostly by T molecules. The structure around a D molecule is quite well defined and independent of temperature, as shown by the temperature independence of the typical energy of the D molecules and by the identity of the radial distribution function g_{DD} up to 4 Å. We finally demonstrate that D molecules, while quite rare at low temperatures, significantly cluster together and that the anomalous behavior of the specific heat is prevalently related to the temperature dependence of the relative concentration of the two molecule types.

SUPPLEMENTARY MATERIAL

See the supplementary material for complementary analysis of the TIP4P/2005 water model, partial RDF calculations, and further C_p^{ex} information.

AUTHORS' CONTRIBUTIONS

J.M.M.O. performed and analyzed the MD simulations. All authors equally contributed to interpreting the data and writing the manuscript.

ACKNOWLEDGMENTS

J.M.M.O. and G.A.A. acknowledge support from CONICET, UNS, and ANPCyT (Grant Nos. PICT2015/1893 and PICT2017/3127). F.S. acknowledges support from MIUR-PRIN 2018 under Grant No. 2017Z55KCW.

DATA AVAILABILITY

The data that support the findings of this study are available from the corresponding author upon reasonable request.

REFERENCES

[1] C. A. Angell, "Amorphous water," Annu. Rev. Phys. Chem. **55**, 559–583 (2004).
[2] C. A. Angell, "Formation of glasses from liquids and biopolymers," Science **267**, 1924–1935 (1995).
[3] O. Mishima and H. E. Stanley, "The relationship between liquid, supercooled and glassy water," Nature **396**, 329 (1998).
[4] P. G. Debenedetti, "Supercooled and glassy water," J. Phys.: Condens. Matter **15**, R1669 (2003).
[5] H. Stanley and P. Debenedetti, "Supercooled and glassy water," Phys. Today **56**(6), 40–46 (2003).
[6] P. H. Poole, F. Sciortino, U. Essmann, and H. E. Stanley, "Phase behaviour of metastable water," Nature **360**, 324 (1992).
[7] P. Gallo, K. Amann-Winkel, C. A. Angell, M. A. Anisimov, F. Caupin, C. Chakravarty, E. Lascaris, T. Loerting, A. Z. Panagiotopoulos, J. Russo *et al.*, "Water: A tale of two liquids," Chem. Rev. **116**, 7463–7500 (2016).
[8] J. Russo and H. Tanaka, "Understanding water's anomalies with locally favoured structures," Nat. Commun. **5**, 3556 (2014).
[9] P. Ball, "Water is an active matrix of life for cell and molecular biology," Proc. Natl. Acad. Sci. U. S. A. **114**, 13327–13335 (2017).
[10] P. H. Handle, T. Loerting, and F. Sciortino, "Supercooled and glassy water: Metastable liquid (s), amorphous solid (s), and a no-man's land," Proc. Natl. Acad. Sci. U. S. A. **114**, 13336–13344 (2017).
[11] H. E. Stanley, *Liquid Polymorphism* (Wiley Online Library, 2013), Vol. 152.
[12] J. C. Palmer, P. H. Poole, F. Sciortino, and P. G. Debenedetti, "Advances in computational studies of the liquid–liquid transition in water and water-like models," Chem. Rev. **118**, 9129–9151 (2018).
[13] F. Sciortino, I. Saika-Voivod, and P. H. Poole, "Study of the ST2 model of water close to the liquid–liquid critical point," Phys. Chem. Chem. Phys. **13**, 19759–19764 (2011).
[14] J. C. Palmer, F. Martelli, Y. Liu, R. Car, A. Z. Panagiotopoulos, and P. G. Debenedetti, "Metastable liquid–liquid transition in a molecular model of water," Nature **510**, 385 (2014).
[15] T. A. Kesselring, G. Franzese, S. V. Buldyrev, H. J. Herrmann, and H. E. Stanley, "Nanoscale dynamics of phase flipping in water near its hypothesized liquid-liquid critical point," Sci. Rep. **2**, 474 (2012).
[16] F. Smallenburg and F. Sciortino, "Tuning the Liquid-Liquid Transition by Modulating the Hydrogen-Bond Angular Flexibility in a Model for Water," Phys. Rev. Lett. **115**, 015701 (2015).
[17] G. E. Walrafen, "Raman spectral studies of the effects of temperature on water structure," J. Chem. Phys. **47**, 114–126 (1967).
[18] A. Nilsson and L. G. M. Pettersson, "Perspective on the structure of liquid water," Chem. Phys. **389**, 1–34 (2011).
[19] A. Taschin, P. Bartolini, R. Eramo, R. Righini, and R. Torre, "Evidence of two distinct local structures of water from ambient to supercooled conditions," Nat. Commun. **4**, 2401 (2013).
[20] K. H. Kim, A. Späh, H. Pathak, F. Perakis, D. Mariedahl, K. Amann-Winkel, J. A. Sellberg, J. H. Lee, S. Kim, J. Park *et al.*, "Maxima in the thermodynamic response and correlation functions of deeply supercooled water," Science **358**, 1589–1593 (2017).
[21] K. Amann-Winkel, C. Gainaru, P. H. Handle, M. Seidl, H. Nelson, R. Böhmer, and T. Loerting, "Water's second glass transition," Proc. Natl. Acad. Sci. U. S. A. **110**, 17720–17725 (2013).
[22] J. N. Stern, M. Seidl-Nigsch, and T. Loerting, "Evidence for high-density liquid water between 0.1 and 0.3 GPa near 150 K," Proc. Natl. Acad. Sci. U. S. A. **116**, 9191–9196 (2019).
[23] A. K. Soper, "Is water one liquid or two?," J. Chem. Phys. **150**, 234503 (2019).
[24] H. Tanaka, H. Tong, R. Shi, and J. Russo, "Revealing key structural features hidden in liquids and glasses," Nat. Rev. Phys. **1**, 333 (2019).
[25] D. C. Malaspina, E. P. Schulz, L. M. Alarcón, M. A. Frechero, and G. A. Appignanesi, "Structural and dynamical aspects of water in contact with a hydrophobic surface," Eur. Phys. J. E **32**, 35–42 (2010).
[26] L. M. Alarcón, D. C. Malaspina, E. P. Schulz, M. A. Frechero, and G. A. Appignanesi, "Structure and orientation of water molecules at model hydrophobic surfaces with curvature: From graphene sheets to carbon nanotubes and fullerenes," Chem. Phys. **388**, 47–56 (2011).
[27] S. R. Accordino, D. C. Malaspina, J. R. Fris, L. Alarcón, and G. Appignanesi, "Temperature dependence of the structure of protein hydration water and the liquid-liquid transition," Phys. Rev. E **85**, 031503 (2012).
[28] E. Shiratani and M. Sasai, "Growth and collapse of structural patterns in the hydrogen bond network in liquid water," J. Chem. Phys. **104**, 7671–7680 (1996).
[29] E. Shiratani and M. Sasai, "Molecular scale precursor of the liquid–liquid phase transition of water," J. Chem. Phys. **108**, 3264–3276 (1998).
[30] G. A. Appignanesi, J. A. Rodriguez Fris, and F. Sciortino, "Evidence of a two-state picture for supercooled water and its connections with glassy dynamics," Eur. Phys. J. E **29**, 305–310 (2009).
[31] S. Accordino, J. R. Fris, F. Sciortino, and G. Appignanesi, "Quantitative investigation of the two-state picture for water in the normal liquid and the supercooled regime," Eur. Phys. J. E **34**, 48 (2011).
[32] D. C. Malaspina, J. A. Rodriguez Fris, G. A. Appignanesi, and F. Sciortino, "Identifying a causal link between structure and dynamics in supercooled water," Europhys. Lett. **88**, 16003 (2009).
[33] J. M. M. de Oca, J. A. R. Fris, S. R. Accordino, D. C. Malaspina, and G. A. Appignanesi, "Structure and dynamics of high- and low-density water molecules in the liquid and supercooled regimes," Eur. Phys. J. E **39**, 124 (2016).
[34] A. R. Verde, J. M. Montes de Oca, S. R. Accordino, L. M. Alarcón, and G. A. Appignanesi, "Comparing the performance of two structural indicators for different water models while seeking for connections between structure and dynamics in the glassy regime," J. Chem. Phys. **150**, 244504 (2019).
[35] I. Saika-Voivod, F. Sciortino, and P. H. Poole, "Computer simulations of liquid silica: Equation of state and liquid–liquid phase transition," Phys. Rev. E **63**, 011202 (2000).
[36] R. Shi and H. Tanaka, "Microscopic structural descriptor of liquid water," J. Chem. Phys. **148**, 124503 (2018).
[37] M. J. Cuthbertson and P. H. Poole, "Mixturelike behavior near a liquid-liquid phase transition in simulations of supercooled water," Phys. Rev. Lett. **106**, 115706 (2011).
[38] F. H. Stillinger, *Energy Landscapes, Inherent Structures, and Condensed-Matter Phenomena* (Princeton University Press, 2015).
[39] F. Sciortino, "Potential energy landscape description of supercooled liquids and glasses," J. Stat. Mech.: Theory Exp. **2005**, P05015.
[40] T. A. Weber and F. H. Stillinger, "Removing chemical bonding ambiguities in condensed media by steepest-descent quenching," J. Chem. Phys. **87**, 3252–3253 (1987).

[41] H. J. C. Berendsen, J. R. Grigera, and T. P. Straatsma, "The missing term in effective pair potentials," J. Phys. Chem. **91**, 6269–6271 (1987).
[42] J. L. F. Abascal and C. Vega, "A general purpose model for the condensed phases of water: Tip4p/2005," J. Chem. Phys. **123**, 234505 (2005).
[43] F. Sciortino and S. L. Fornili, "Hydrogen bond cooperativity in simulated water: Time dependence analysis of pair interactions," J. Chem. Phys. **90**, 2786–2792 (1989).
[44] S. Saito, B. Bagchi, and I. Ohmine, "Crucial role of fragmented and isolated defects in persistent relaxation of deeply supercooled water," J. Chem. Phys. **149**, 124504 (2018).
[45] J. Finney, A. Hallbrucker, I. Kohl, A. Soper, and D. Bowron, "Structures of high and low density amorphous ice by neutron diffraction," Phys. Rev. Lett. **88**, 225503 (2002).
[46] J.-P. Hansen and I. R. McDonald, *Theory of Simple Liquids* (Elsevier, 1990).